Full Text View

Volume 28, Issue 11 (November 1998)

Journal of Physical Oceanography
Article: pp. 2313–2331 | Abstract | PDF (317K)

Transport and Resuspension of Fine Particles in a Tidal Boundary Layer near a Small Peninsula

Chiang C. Mei, Chimin Chian, and Feng Ye

Department of Civil and Environmental Engineering, Massachusetts Institute of Technology, Cambridge, Massachusetts

(Manuscript received June 16, 1997, in final form January 20, 1998)
DOI: 10.1175/1520-0485(1998)028<2313:TAROFP>2.0.CO;2

ABSTRACT

The authors present a theory on the transport and resuspension of fine particles in a tidal boundary layer when the ambient tidal flow is nonuniform due to a peninsula along the coastline. As a first step toward better physical understanding the authors adopt the model of constant eddy viscosity and a horizontal seabed. Attention is focused on a peninsula whose horizontal dimension is much smaller than the tidal wave length but larger than the tidal excursion length. General expressions of shear-induced dispersivities and convection velocity are derived in terms of the ambient flow field. Nonuniformity in the horizontal flow is found to have profound effects on the spatial variation of the dispersion tensor as well as the horizontal convection velocity. Two numerical examples are given for a semicircular peninsula: one for a particle cloud released near the peninsula over a nonerodible seabed, and one for the resuspension over an erodible belt around the peninsula.

1. Introduction

Transport of suspended sediments in coastal waters is of importance to coastline evolution and has been the subject of investigation for a long time. Recent interest has been motivated by environmental concerns of coastal waste disposal and the ecological processes of larvae birth and growth.

Dispersion of a neutrally buoyant cloud in a horizontally uniform oscillatory current has been studied by a number of authors (e.g., Bowden 1965; Holly and Harleman 1965; Okubo 1967; Fukuoka 1974). For the dispersion of heavy particles, Yasuda (1989) also gave a theory for an oscillating horizontally uniform current within a Stokes boundary layer. The effective dispersivity at the final stationary stage was found to depend on the fall velocity of the particles. Carter and Okubo (1965) investigated a straight channel flow with linear variation of velocity in the two transverse directions and obtained solutions for the concentration distribution of a neutrally buoyant cloud. Although many important physical features have been revealed, these studies are applicable only when the sediment cloud size and the distance of advection are much smaller than the horizontal scale of the mean flow. If one is interested in the long-time fate of a particular cloud with horizontal dimensions comparable to the length scale of an estuary, a nearby island or a peninsula, the uniform-tide theories cannot be satisfactory.

For the mixing and flushing of tidal embayments in the Dutch Wadden Sea, Zimmerman (1976, 1977) found that the large diffusivity (100–1000 $m^2\ s^{-1}$) is attributable to horizontal mixing in a spatially varying flow. Since then a number of papers have addressed the effect of horizontal variation of bathymetry or topography on advection and dispersion.

There have been two approaches to model mixing in nonuniform tides. One is to compute the depth-averaged flow first. Then the trajectories (or Stokes drift) of a large number of marked fluid particles are computed numerically as an Euler–Lagrange problem (Zimmerman 1986). If the computed time history is sufficiently long, the particle paths of this Stokes drift become chaotic. Effective diffusivity is then calculated from the variance of the particle separation. Using this approach Awaji et al. (1980) and Awaji (1982) studied the tidal mixing in an idealized strait. Signell and Geyer (1990) studied a similar problem for a peninsula that is small compared to the tidal excursion length so that separation eddies are a dominant feature. The second approach, taken by Young et al. (1982) is Eulerian. They examined an idealized flow field with simple dependence on depth and horizontal coordinates, and sinusoidal dependence in time. The three-dimensional convective diffusion problem was solved to enable the calculation of the effective horizontal diffusivity.

In this paper we extend the Eulerian approach to dispersion in tidal flows affected strongly by nonuniformities due to coastal topography. Our main assumptions are as follows. The topographical length scale is assumed to be greater than the tidal excursion length so that flow separation is not important. Let h denote the sea depth, r_o the horizontal size of the coastal topography, A the typical tide amplitude, ω the tidal frequency, and $\mathcal{U} \sim A(gh)^{1/2}/h$ the typical horizontal flow velocity.[1] Just above the seabed, an oscillatory Ekman boundary layer of the thickness $\delta = O((\nu_e/\omega)^{1/2})$ is expected to develop, where ν_e denotes the eddy viscosity of momentum. The various scales involved in this problem are assumed to satisfy the following constraints:

$$\epsilon \equiv \frac{\mathcal{U}}{\omega r_o} \ll 1, \qquad \frac{\delta}{h} \ll 1,$$

$$\frac{h}{r_o} \ll 1, \qquad kr_o \ll 1. \qquad (1.1)$$

They mean, respectively, that the tidal excursion is small compared to the island size, the Ekman layer is totally submerged near the sea bottom beneath the inviscid zone, the sea is very shallow compared to the topographical length scale, which is in turn very small relative to the tidal wave length $2\pi/k$. In addition, we shall model the resuspension of fine particles from the seabed by the usual empirical formula that the erosion rate is a function of the shear stress at the seabed (Krone 1962;Partheniades 1965) and assume that the heavy particles are kept in suspension by flow turbulence in the tidal boundary layer. Formation of agregates of cohesive sediments is not considered.

The conditions of Eq. (1.1) are easily met. Taking for estimate the tidal amplitude A = 1.75 m, average depth h = 30 m, then $\mathcal{U} = A(gh)^{1/2}/h$ = 1 m s^{-1}. Let the tidal period be 12 h so that $\omega = 2\pi/12$ (1/h) = 1.45 × 10^{-4} (1/s), and the radius be r_o = 50 km, then $\epsilon = \mathcal{U}/(\omega r_o)$ = 0.138 and is small.

Concerning the eddy viscosity, there have been many depth-dependent models in the literature of gravity waves (Sleath 1990) and of tidal currents (Soulsby 1990). It is known that despite the varieties of models (constant, linear, parabolic, exponential), the resulting first-order velocity profiles do not differ qualitatively (see, e.g., Soulsby 1990, p. 531). For achieving analytical results, we shall choose the simplest model of constant eddy viscosity with no-slip boundary at the seabed (Sverdrup 1927; Mofjeld 1980; Kundu et al. 1981; and Fang and Ichiye 1983). To help guide the estimate of order of magnitudes we use the usual assumption (Soulsby 1983)

$$\nu_e = \kappa u* z, \qquad (1.2)$$

where κ = 0.4 is the von Kármán constant and $u* = (\tau_b/\rho)^{1/2}$ is the friction velocity, which depends on the local shear stress at the bed. As estimates we may take $u*$ = 1 cm s^{-1} for a smooth mud bed and $u*$ = 2.5 cm s^{-1} for a rippled sandy bed (Soulsby 1983, p. 196), then for a tidal boundary layer of depth 10 m, ν_e = 0.02–0.05 $m^2\ s^{-1}$, which is consistent with the estimates by Bowden and Fairbairn (1953). Clearly (1.2) implies that the eddy viscosity is a function of local flow, but its full use would require a considerable numerical task, which is not attempted here.

Under our simplifying assumptions, we take advantage of two features of the phenomenon: (i) the existence of two vastly different timescales (time for vertical diffusion across the sea bed boundary layer and time for horizontal diffusion across the topographical length) and (ii) the problem is periodic on the shorter (micro) timescale, which is just the tidal period. These features enable us to employ the perturbation method of multiple scales (method of homogenization) for deriving the effective equation governing the horizontal convection and dispersion of the particle concentration. Both the dispersivities and convection velocities will be derived for general flow patterns with significant spatial variations produced by the interaction of tides with lateral boundaries. The analysis is an extension to our earlier works on gravity waves over a nonerodible seabed (Mei and Chian 1994) and an erodible seabed (Mei et al. 1997) without Coriolis effects.

2. Flow in the tidal boundary layer

Under the second assumption in Eq. (1.1), the boundary layer equations can be written:

$$\frac{\partial \mathbf{u}}{\partial t} + \mathbf{u}\cdot\nabla\mathbf{u} + w\frac{\partial \mathbf{u}}{\partial z} + 2\Omega \times \mathbf{u} - \nu_e\frac{\partial^2 \mathbf{u}}{\partial z^2} = \frac{\partial \mathbf{U}_I}{\partial t} + \mathbf{U}_I\cdot\nabla\mathbf{U}_I + 2\boldsymbol{\Omega} \times \mathbf{U}_I, \qquad (2.1)$$

where $\mathbf{u} = (u, v)$ denotes the horizontal velocity vector, w the vertical velocity component, ν_e the eddy viscosity, and $\boldsymbol{\Omega} = \Omega\mathbf{k}$ is the local angular velocity of the earth rotation, with $\Omega = 2\pi \sin\Phi$/day and Φ being the local latitude; $\mathbf{U}_I$ denotes the horizontal velocty of the inviscid flow field just outside the boundary layer,

$$\mathbf{U}_I = \mathrm{Re}[\mathbf{U}_0(x, y)e^{-i\omega t}] = \frac{1}{2}(\mathbf{U}_0 e^{-i\omega t} + \mathbf{U}_0^* e^{i\omega t}), \qquad (2.2)$$

where asterisks signify complex conjugates.

The first assumption in Eq. (1.1) permits one to expand the velocity in the boundary layer as

$$\mathbf{u} = \mathbf{u}^{(1)} + \mathbf{u}^{(2)} + \cdots,$$

where the superscripts indicate the order of magnitude in powers of ϵ. At the leading order, the horizontal momentum equation reads

$$\frac{\partial \mathbf{u}^{(1)}}{\partial t} + 2\Omega \times \mathbf{u}^{(1)} - \nu_e\frac{\partial^2 \mathbf{u}^{(1)}}{\partial z^2} = \frac{\partial \mathbf{U}_I}{\partial t} + 2\boldsymbol{\Omega} \times \mathbf{U}_I. \qquad (2.3)$$

The first-order horizontal velocity in the bottom boundary layer was given first by Hunt and Johns (1963) as follows:

$$u^{(1)} = \mathrm{Re}[(U_0F_1 - V_0F_2)e^{-i\omega t}], \qquad (2.4)$$

$$v^{(1)} = \mathrm{Re}[(U_0F_2 + V_0F_1)e^{-i\omega t}] \qquad (2.5)$$

in which

$$F_1 = 1 - \frac{1}{2}(e^{-s\xi} + e^{-q\xi}), \qquad (2.6)$$

$$F_2 = \frac{i}{2}(e^{-s\xi} - e^{-q\xi}), \qquad (2.7)$$

where

$$q = (1 - i)\alpha, \qquad (2.8)$$

$$s = (1 \mp i)\beta, \quad \text{if } f \lessgtr 1 \qquad (2.9)$$

$$\alpha = \sqrt{1 + f}, \qquad \beta = \sqrt{|1 - f|}, \qquad f = 2\Omega/\omega, \qquad (2.10)$$

and

$$\xi = \frac{z}{\delta}, \qquad \delta = \sqrt{\frac{2\nu_e}{\omega}}. \qquad (2.11)$$

As has been shown by Buchwald (1971) that under the last two assumptions in Eq. (1.1), the inviscid tidal flow (U_I, V_I) can be described essentially by a two-dimensional, quasi-steady velocity potential, while the vertical velocity component is negligible. In particular,

$$\frac{\partial U_I}{\partial x} + \frac{\partial V_I}{\partial y} = O(kr_o)^2\left(\frac{\mathcal{U}}{r_o}\right),$$

$$\frac{\partial U_I}{\partial y} - \frac{\partial V_I}{\partial x} = O(kr_o)^2\left(\frac{\mathcal{U}}{r_o}\right). \qquad (2.12)$$

It follows readily from continuity that the vertical velocity in the boundary layer is of the order

$$\frac{\delta}{r_o}(kr_o)^2\frac{\mathcal{U}}{r_o} \qquad (2.13)$$

and is negligible (Lamoure and Mei 1977). As a further consequence the spatial factors U_0 and V_0 are in phase and may be taken as real quantities with respect to i. Based on these Lamoure and Mei have solved the approximate momentum equation at second order, $O(\epsilon)$,

$$\frac{\partial \mathbf{u}^{(2)}}{\partial t} + 2\Omega \times \mathbf{u}^{(2)} - \nu_e\frac{\partial^2 \mathbf{u}^{(2)}}{\partial z^2} = \mathbf{U}_I\cdot\nabla\mathbf{U}_I - \mathbf{u}^{(1)}\cdot\nabla\mathbf{u}^{(1)}$$

$$= \frac{1}{2}\nabla(\mathbf{U}_I^2 - \mathbf{u}^{(1)^2}). \quad (2.14)$$

The period average of $\mathbf{u}_2$ gives the Eulerian streaming induced by Reynolds stresses in the tidal boundary layer. Using real notation, the second-order-induced streaming is given by

$$\langle u^{(2)}\rangle = \frac{1}{2\omega}\left\{\mathrm{Re}H_E(\xi)\frac{\partial}{\partial x}|\mathbf{U}_0|^2 - \mathrm{Im}H_E(\xi)\frac{\partial}{\partial y}|\mathbf{U}_0|^2\right\} \quad (2.15)$$

$$\langle v^{(2)}\rangle = \frac{1}{2\omega}\left\{\mathrm{Im}H_E(\xi)\frac{\partial}{\partial x}|\mathbf{U}_0|^2 + \mathrm{Re}H_E(\xi)\frac{\partial}{\partial y}|\mathbf{U}_0|^2\right\}, \quad (2.16)$$

where

$$|\mathbf{U}_0| = (|U_0|^2 + |V_0|^2)^{1/2}; \quad (2.17)$$

angle brackets denote time averages over a tidal period, and $H_E(\xi)$ marks the vertical variation of Eulerian streaming in the boundary layer

$$-H_E = \frac{1}{2}\left\{-\left(\frac{1}{q^2 - c^2} + \frac{1}{q^{*2} - c^2} - \frac{1}{4\alpha^2 - c^2}\right)e^{-c\xi} + \frac{1}{q^2 - c^2}e^{-q\xi} + \frac{1}{q^{*2} - c^2}e^{-q^*\xi} - \frac{1}{4\alpha^2 - c^2}e^{-2\alpha\xi}\right\}$$

$$+ \frac{1}{2}\{\alpha \to \beta,\ q \to s\}, \qquad (2.18)$$

(Click the equation graphic to enlarge/reduce size)

where

$$c = (1 + i)(f)^{1/2}. \quad (2.19)$$

In Eq. (2.18) the expression in the second pair of braces is obtained from the first pair by the indicated change of parameters. This result has been derived and discussed by Lamoure and Mei.

3. Governing equation for particle transport

Consider a dilute cloud of fine particles either released from a dredge boat or resuspended locally from an erodible bed. In general, the sediment size is distributed over a certain range. Since for a dilute cloud interaction among particles is negligible, one can divide the size distribution into a discrete set of particle sizes, each of which is characterized by a fall velocity w_o.

After analyzing the concentration of each size, the evolution of the entire cloud can be obtained by linear superposition. In the sequel only one size is considered.

We first give reasons that the inertia of sufficiently small particles can be ignored. The ratio of the relaxation time τ for a particle to adjust to the ambient mean flow to that of the tidal wave period can be estimated by

$$\omega\tau = \frac{4d\rho_p g\omega}{3C_D\Delta u} \qquad (3.1)$$

(Bagnold 1951) with d, ρ_p, C_D, and Δu being respectively the diameter and density of the particle, the drag coefficient, and the representative initial velocity difference between a particle and the ambient fluid. With $C_D = O(1)$ and $\Delta u = O(1)$ m s^{-1}, this ratio is about $O(10^{-5})$ for $d = O(0.1)$ mm = 100 μm (fine sand) and is very small so that the particles are essentally inertia free. In a turbulent field, fine particles can also be considered inertia free relative to turbulent fluctuations if they are small compared to the Kolmogorov length, $l_k = (\nu^3 l/u'^3)^{1/4}$, which is the smallest length scale of viscous eddies; that is,

$$\frac{d}{l_k} < O(1), \qquad (3.2)$$

where ν is the molecular viscosity of water, l is the eddy size, and u' the velocity scale of turbulent fluctuations. It is reasonable to use the boundary layer thickness δ as the scale of l and friction velocity $u* = \tau_b/\rho$ as the scale of u', where τ_b stands for the bed shear stress. Estimating the tidal boundary layer thickness to be l = 10 m and $u* = O(0.01)$ m s^{-1}, we have $l_k = O(1.8)$ mm, which is much greater than the diameter of fine sand. We shall, therefore, ignore the velocity difference between the particle and its surrounding fluid.

Let D and D_h be the vertical and horizontal eddy mass diffusivities respectively. The convection–diffusion equation for the concentration C of a dilute particle cloud can be approximated by

$$\frac{\partial C}{\partial t} + \frac{\partial u_i C}{\partial x_i} + \frac{\partial (w - w_o)C}{\partial z} = D_h \frac{\partial^2 C}{\partial x_i \partial x_i} + D\frac{\partial^2 C}{\partial z^2}, \qquad (3.3)$$

where i = 1, 2 corresponding to the two horizontal coordinates.

From the experiments by Krone (1962) and Partheniades (1965) for steady flow over an erodible bed, the net rate of erosion or deposition of cohesive sediments is related to the excess of bed shear stress above a threshold stress. In its simplest form it reads

$$-w_0 C - D\frac{\partial C}{\partial z} = \begin{cases} -\mathcal{D} \\ \mathcal{E} \end{cases} \quad \text{if} \begin{cases} |\tau_b| < \tau_d \\ |\tau_b| > \tau_c \end{cases}, \qquad (3.4)$$

where $\tau_c > \tau_d$ and

$$\mathcal{D} = \alpha_d w_d C \qquad (3.5)$$

represents the rate of deposition, w_d is the deposition velocity, α_d is an empirical coefficient no greater than unity, and

$$\mathcal{E} = E(|\tau_b| - \tau_c) \qquad (3.6)$$

represents the rate of erosion while E is another empirical coefficient. Normally τ_d ranges from 0.03~0.15 N m^{-2} for various types of sediments, while τ_c lies between 0.15 N m^{-2} and 1 N m^{-2}; see Tables 11.3, 11.7, and 11.8 in van Rijn (1994). The surface layer of the seabed is usually covered with partially consolidated or unconsolidated particles for which τ_c is considerably less than the bed shear stress in the tidal wave boundary layer, namely, $|\tau_b| \gg \tau_c$. Thus, we shall neglect τ_c as well as τ_d ($<\tau_c$) and approximate Eq. (3.4) by

$$-\left(w_0 C + D\frac{\partial C}{\partial z}\right) = \mathcal{E} \approx E|\tau_b|, \qquad z = 0. \qquad (3.7)$$

Furthermore, in a steady turbulent flow, particles, once suspended, can remain in suspension without deposition if $w_0/\kappa u_* < O(1)$ (Batchelor 1965), where u_* and κ are the bottom shear velocity and the von Kármán constant, respectively. As an estimate let us take $u_* = O(0.01)$ m s^{-1}, then the above condition is satisfied for $w_o > O(0.004)$ m s^{-1}, which corresponds to a sand size $d = O(0.1)$ mm or finer. In any case, inclusion of the small effects of τ_d and τ_c is merely cumbersome but not difficult.

Because sand particles are heavier than water, they are kept in suspension by the flow turbulence, hence are essentially confined inside the tidal boundary layer. We therefore assume that C vanishes at the upper edge of the boundary layer

$$C = 0, \qquad z \longrightarrow \infty. \tag{3.8}$$

4. Scaling and normalization

There are three vertical length scales pertinent to the boundary layer:

$$\delta_s = D/w_0, \delta_u = (2\nu_e/\omega)^{1/2}, \delta_c = (2D/\omega)^{1/2}. \tag{4.1}$$

Here δ_s denotes the thickness of a steady concentration layer resulting from the settling of particles and the upward turbulent diffusion, and δ_u and δ_c are the boundary layer thicknesses corresponding to momentum and mass diffusion, respectively. For generality we shall assume that all three scales are comparable to one another and therefore characterized by a single scale δ; that is,

$$O(\delta) = O(\delta_s) = O(\delta_u) = O(\delta_c). \tag{4.2}$$

and thus the Schmidt number is of order unity.

$$\mathrm{Sc} = \nu_e/D = (\delta_u/\delta_c)^2 = O(1). \tag{4.3}$$

Indeed, if Reynolds analogy is assumed, $\mathrm{Sc} = \nu_e/D$ is precisely unity.

Two small length ratios are crucial in this study. Compared to the horizontal dimension of the peninsula,

$$\epsilon = \frac{\mathcal{U}}{\omega r_0} = \frac{A\sqrt{gh}}{r_o}, \tag{4.4}$$

is a measure of the tidal excursion length, and

$$\epsilon_1 = \frac{\delta}{r_0}\sqrt{\frac{D_h}{D}}, \tag{4.5}$$

where ϵ_1 is a dimensionless measure of the boundary layer thickness. We shall assume that $O(\epsilon_1) \leqslant O(\epsilon)$, the consequence of which is that horizontal turbulent diffusion will remain effective in the long-term transport of sediment concentration. Estimating $D_h/D = 10^4$, $\delta = 10$ m, and $r_0 = 50\ 000$ m, we get $\epsilon_1 = 0.02$, which is much smaller than ϵ; hence our assumption is a generous one.

Let us introduce the normalized variables as follows:

$$x_i = r_o x_i^*, \qquad z = \delta z^*, \qquad t = \frac{t^*}{\omega},$$

$$C = C_0 C^*, \qquad u_i = \mathcal{U} u_i^*, \qquad w = \frac{\delta}{r_0}\mathcal{U} w^*. \tag{4.6}$$

In dimensionless form, the governing equation reads, with the asterisks omitted for brevity,

(4.7)

where Pe = $w_0\delta/D$ is the particle Péclet number and $z^* = \xi$ by definition.

As shown by Mei et al. (1997), the characteristic concentration C_0 can be estimated by balancing the rate of erosion and the net horizontal flux by Eulerian streaming within the boundary layer, namely,

$$\mathcal{U}_E \delta \frac{\partial C}{\partial x} \sim E\tau_b, \qquad (4.8)$$

where $\mathcal{U}_E$ denotes the scale of the Eulerian steady streaming. From (2.15) and (2.16) we can estimate

$$\mathcal{U}_E = O\left(\frac{\mathcal{U}^2}{\omega r_0}\right). \qquad (4.9)$$

where $\mathcal{U} = A(gh)^{1/2}/h$ for long waves in shallow seas; hence

$$E\tau_0 \sim \frac{\delta A^2 g C_0}{\omega h r_0^2}. \qquad (4.10)$$

The shear stress on the sea bottom can be estimated from the boundary layer theory as

$$\tau_0 = \frac{\sqrt{2}\,\rho D\mathcal{U}}{\delta} = \frac{\sqrt{2g}\,\rho DA}{\delta\sqrt{h}}; \qquad (4.11)$$

therefore

$$C_0 \sim \frac{\sqrt{2}\,\rho E D\omega r_0^2\sqrt{h}}{A\delta^2\sqrt{g}} \sim \frac{\sqrt{2}\,\rho DE\omega r_0^2}{\delta^2\mathcal{U}}. \qquad (4.12)$$

Using this, the normalized boundary condition at the seabed reads

$$-\mathrm{Pe}C - \frac{\partial C}{\partial z} = \frac{\mathcal{U}^2\delta^2}{\omega D r_0^2}|\tau_b|, \qquad (4.13)$$

where

$$\frac{\mathcal{U}^2\delta^2}{\omega D r_0^2} \sim \frac{A^2}{r_o}\frac{\delta^2\omega}{D} = O(\epsilon^2). \qquad (4.14)$$

This scale estimate is consistent with field observations by Huhe and Yang (1996), Yu et al. (1993), and cited by Mei et al. (1997).

In the present problem there are two timescales: One is $\omega^{-1} = T/2\pi = O(\delta^2/D)$, which characterizes the vertical diffusion across the boundary layer. The other is the timescale for horizontal transport by convection across the peninsula, $r_0/\langle u^{(2)}\rangle$; the timescale for horizontal diffusion $r^2{}_0/D_h$ is much longer and immaterial. Using either Eq. (2.15) or Eq. (2.16) we get $\langle u^{(2)}\rangle = O(\mathcal{U}^2/\omega r_0)$. Therefore, the timescale for horizontal transport is $r^2{}_0\omega/\mathcal{U}^2$. The ratio between two timescales for vertical and horiontal transport is $O(\epsilon^2)$. Accordingly we may introduce a slow time variable $T = \epsilon^2 t$.

5. Effective equation for horizontal particle transport

With these order estimates it is possible to return to physical coordinates by keeping the order symbols in order to mark the relative magnitudes. Thus, we have

$$= D\frac{\partial^2 C}{\partial z^2} + \epsilon^2 D_h \frac{\partial^2 C}{\partial x_i \partial x_i}, \qquad (5.1)$$

$$-\left(w_0 C + D\frac{\partial C}{\partial z}\right) = \epsilon^2 E|\tau_b|, \qquad z = 0, \qquad (5.2)$$

$$C \to 0, \qquad z \gg \delta. \qquad (5.3)$$

As in Mei and Chian (1994) and Mei et al. (1997), we employ multiple-scale expansions

$$C = C^{(0)}(x_i, z, T) + \epsilon C^{(1)}(x_i, z, t, T) + \epsilon^2 C^{(2)}(x_i, z, t, T) + O(\epsilon^3). \qquad (5.4)$$

At the leading order $O(1)$, the equation is quasi-steady and homogeneous.

$$\frac{\partial}{\partial z}\left(w_0 C^{(0)} + D\frac{\partial C^{(0)}}{\partial z}\right) = 0, \qquad (5.5)$$

subject to the homogeneous boundary conditions

$$w_0 C^{(0)} + D\frac{\partial C^{(0)}}{\partial z} = 0 \qquad (5.6)$$

$$C^{(0)} = 0 \qquad z = \infty. \qquad (5.7)$$

Thus, the solution,

$$C^{(0)} = \hat{C}(x_i, T)e^{-\mathrm{Pe}\xi}, \qquad (5.8)$$

represents the time-averaged concentration, whose dependence on x_i, T through the factor $\hat{C}(x_i, T)$ is yet unknown.

At $O(\epsilon)$, we have the equation for the concentration fluctuation $C^{(1)}$ from the mean.

$$\frac{\partial C^{(1)}}{\partial t} - \frac{\partial}{\partial z}\left(w_0 C^{(1)} + D\frac{\partial C^{(1)}}{\partial z}\right) = -u_i^{(1)}\frac{\partial C^{(0)}}{\partial x_i}, \qquad (5.9)$$

subject to the same boundary conditions, Eqs. (5.6) and (5.7). In Eq. (5.9) we have dropped the term $w_1 \partial C^{(0)}/\partial z$ because w_1 is negligible near a small peninsula, as pointed out before in section 2. Let

$$C^{(1)} = \mathrm{Re}\, C_{11} e^{-i\omega t}. \qquad (5.10)$$

Using the solutions for u_{1i} as given in Eqs. (2.4) and (2.5), the formal solution for $C^{(0)}$, and the boundary conditions for $C^{(1)}$ we obtain

$$C_{11} = \frac{1}{\omega}[(R_1 U_0 - R_2 V_0)e^{A_1 \mathrm{Pe}\xi} + R_3 U_0 e^{-\mathrm{Pe}\xi} + R_\alpha (U_0 - iV_0)e^{-A_\alpha \mathrm{Pe}\xi} + R_\beta (U_0 + iV_0)e^{-A_\beta \mathrm{Pe}\xi}]\frac{\partial C}{\partial x} + \frac{1}{\omega}[U_0 \to V_0, V_0 \to -U_0]\frac{\partial C}{\partial y}, \qquad (5.11)$$

with

$$R_1 = -\frac{\mathrm{Sc}}{\mathrm{Pe}^2(A_1 + 1)}\left[\frac{A_\beta - 1}{(A_1 + A_\beta)(A_2 + A_\beta)} + \frac{A_\alpha - 1}{(A_1 + A_\alpha)(A_2 + A_\alpha)}\right], \quad (5.12)$$

$$R_2 = \frac{i\mathrm{Sc}(A_\alpha - A_\beta)}{\mathrm{Pe}^2(A_1 - A_2)}\left[-\frac{1}{(A_1 + A_\alpha)(A_1 + A_\beta)} + \frac{A_2 + 1}{(A_2 + A_\alpha)(A_2 + A_\beta)(A_1 + 1)}\right], \quad (5.13)$$

$$R_3 = -i = \frac{2\mathrm{Sc}}{\mathrm{Pe}^2(1 + A_1)(1 + A_2)}, \quad (5.14)$$

$$R_{\alpha,\beta} = -\frac{\mathrm{Sc}}{\mathrm{Pe}^2(A_1 + A_{\alpha,\beta})(A_2 + A_{\alpha,\beta})}, \quad (5.15)$$

$$A_\alpha = (1 - i)\alpha/\mathrm{Pe} + 1, \quad (5.16)$$

$$A_\beta = (1 - i)\beta/\mathrm{Pe} + 1,$$

$$A_{1,2} = -\frac{1}{2}(1 \pm \Gamma_1) \pm \frac{1}{2}i\Gamma_2, \quad (5.17)$$

$$\Gamma_{1,2} = \left[\frac{\sqrt{(1 + N^4)} \pm 1}{2}\right]^{1/2}, \quad (5.18)$$

$$N = \frac{2\sqrt{2\mathrm{Sc}}}{\mathrm{Pe}}, \qquad \mathrm{Pe} = \frac{w_0\delta}{D}, \qquad \mathrm{Sc} = \frac{\nu_e}{D}. \quad (5.19)$$

Note that Pe is the particle Péclet number, which increases with the particle fall velocity, hence its diameter;Sc is the Schmitt number measuring the ratio of momentum and mass diffusivities.

At $O(\epsilon^2)$ $C^{(2)}$ is governed by

$$\frac{\partial C^{(2)}}{\partial t} + \frac{\partial}{\partial z}\left(-w_0 C^{(2)} - D\frac{\partial C^{(2)}}{\partial z} + w^{(1)}C^{(1)} + w^{(2)}C^{(0)}\right) = -u_i^{(1)}\frac{\partial C^{(1)}}{\partial x_i} - \frac{\partial C^{(0)}}{\partial T} - u_i^{(2)}\frac{\partial C^{(0)}}{\partial x_i} + D_h\frac{\partial^2 C^{(0)}}{\partial x_i \partial x_i}. \quad (5.20)$$

Taking time average and integrating across the boundary layer and noting that the concentration vanishes at the top of the layer and that the vertical velocity must be zero at the bottom, we get the effective transport equation for C:

$$= -\frac{\partial}{\partial x_i}\overline{\langle u_i^{(1)} C^{(1)}\rangle} + D_h \overline{F}\frac{\partial^2 \hat{C}}{\partial x_i \partial x_i} + E\langle|\tau_b|\rangle, \quad (5.21)$$

where overbars denote vertical integration across the boundary layer and $F = e^{-\mathrm{Pe}\xi}$. Using the results Eqs. (2.4), (2.5), (5.11), and (2.15), we finally have the following effective transport equation:

$$\frac{\partial \hat{C}}{\partial T} + \frac{\partial}{\partial x_1}(U_{Ei}\hat{C}) = \frac{\partial}{\partial x_i}\left[(E_{i,j} + D_h\delta_{ij})\frac{\partial \hat{C}}{\partial x_j}\right] + \frac{E\mathrm{Pe}\langle|\tau_b|\rangle}{\delta}, \quad (5.22)$$

The effective convection velocity $\mathbf{U}_E$ has the components

$$\begin{Bmatrix} U_{E_1} \\ U_{E_2} \end{Bmatrix} = \frac{1}{2\omega}\begin{Bmatrix} \frac{\partial}{\partial x} \\ \frac{\partial}{\partial y} \end{Bmatrix}(|U_0|^2 + |V_0|^2)\mathrm{Re}(H_1) + \frac{1}{2\omega}\begin{Bmatrix} -\frac{\partial}{\partial y} \\ \frac{\partial}{\partial x} \end{Bmatrix}(|U_0|^2 + |V_0|^2)\mathrm{Im}(H_1), \quad (5.23)$$

where

$$H_1 = G(\alpha) + G(\beta) \quad (5.24)$$

with

$$G(\alpha) = \mathrm{Pe}\left[\frac{I_1(\alpha)}{c + \mathrm{Pe}} + \frac{I_2(\alpha)}{q + \mathrm{Pe}} + \frac{I_3(\alpha)}{q^* + \mathrm{Pe}} + \frac{I_4(\alpha)}{2\alpha + \mathrm{Pe}}\right], \quad (5.25)$$

and

$$I_1(\alpha) = \frac{1}{4(\alpha^2 + f)i} - \frac{1}{4(\alpha^2 - f)i} + \frac{1}{8\alpha^2 - 4fi}, \quad (5.26)$$

$$I_2(\alpha) = -\frac{1}{4(\alpha^2 + f)i}, \quad (5.27)$$

$$I_3(\alpha) = \frac{1}{4(\alpha^2 - f)i}, \quad (5.28)$$

$$I_4(\alpha) = -\frac{1}{8\alpha^2 - 4fi}. \quad (5.29)$$

Recall that $\alpha(f)$ and $\beta(f)$ are defined in Eq. (2.10), while $q(f)$ and $c(f)$ are defined in Eqs. (2.8) and (2.19) respectively. The polar plot of complex coefficient H_1 is presented in Fig. 1 for a wide range of f. Referring to (5.23), the effecive convection velocity field is the weighted depth average of the Eulerian streaming velocity, proportional to the Reynolds stress imposed by convective inertia in the inviscid flow above the boundary layer. The complex factor H_1 combines the effects of shear and the concentration variation F inside the boundary layer. The ratio $\mathrm{Im}H_1/\mathrm{Re}H_1 = \tan^{-1}\theta_H$ gives the angle θ_H between the driving external Reynolds stress and the convection current, as a result of earth rotation. Thus, for $f - 0$, $\mathrm{Im}H_1$

= 0 so that the angle is zero. But as f increases to 1, the convection velocity is inclined at 67° clockwise from the external Reynolds stress. For f increasing past unity, the angle θ_H decreases again.

The dispersion tensor is in general nonsymmetric and has the components

$$E_{xx} = \frac{1}{\omega}\mathrm{Re}[H_{41}|U_0|^2 + H_{42}|V_0|^2 + H_{43}U_0^* V_0 + H_{44}V_0^* U_0], \tag{5.30}$$

$$E_{yy} = \frac{1}{\omega}\mathrm{Re}[H_{41}|V_0|^2 + H_{42}|U_0|^2 - H_{44}U_0^* V_0 + H_{43}V_0^* U_0], \tag{5.31}$$

$$E_{xy} = \frac{1}{\omega}\mathrm{Re}[-H_{43}|U_0|^2 + H_{44}|V_0|^2 + H_{41}U_0^* V_0 - H_{42}U_0 V_0^*], \tag{5.32}$$

$$E_{yx} = \frac{1}{\omega}\mathrm{Re}[H_{43}|V_0|^2 - H_{44}|U_0|^2 + H_{41}U_0 V_0^* - H_{42}U_0^* V_0]. \tag{5.33}$$

Note that all these components depend quadratically on the ambient velocity components. Moreover, the coefficients

$$H_{41} = -\frac{1}{2}[R_1 S_1(A_1) + R_3 S_1(-1) + R_\alpha S_1(-A_\alpha) + R_\beta S_1(-A_\beta)], \tag{5.34}$$

$$H_{42} = -\frac{1}{2}[R_2 S_2(A_1) + iR_\alpha S_2(-A_\alpha) - iR_\beta S_2(-A_\beta)], \tag{5.35}$$

$$H_{43} = \frac{1}{2}[R_2 S_1(A_1) + iR_\alpha S_1(-A_\alpha) - iR_\beta S_1(-A_\beta)], \tag{5.36}$$

$$H_{44} = \frac{1}{2}[R_1 S_2(A_1) + R_3 S_2(-1) + R_\alpha S_2(-A_\alpha) + R_\beta S_2(-A_\beta)], \tag{5.37}$$

$$S_1(a_i) = \mathrm{Pe}\frac{2a_i\mathrm{Pe} - (s^* + q^*)}{2(a_i\mathrm{Pe} - q^*)(a_i\mathrm{Pe} - s^*)} - \frac{1}{a_i}, \tag{5.38}$$

$$S_2(a_i) = \mathrm{Pe}\frac{i(s^* - q^*)}{2(a_i\mathrm{Pe} - q^*)(a_i\mathrm{Pe} - s^*)}, \tag{5.39}$$

in which $\{a_1, a_2, a_3, a_4\} = \{A_1, -1, -A_\alpha, -A_\beta\}$, represent the integrated effects of the vertical variation of the fluctuating velocity and concentration inside the Ekman boundary layer, hence the coefficients H_{4i}, $i = 1, 2, 3, 4$, are functions of f, Sc, and Pe. Since U_0, V_0 are in phase and can be taken as real numbers, only the real parts of H_{4i} are needed, and are plotted in Fig. 2 as functions of the particle Péclet number Pe for and three different values of Sc. To represent midlatitudes we select $f = 0.666$, which corresponds to the Italian peninsula of Prom. del Gargano[2] at latitude 41°50′ on the southwest coast of the Adriatic Sea.

The magnitudes of all of these coefficients achieve their greatest values near Pe ≈ 1. Dependence of these coefficients on f is plotted in Fig. 3 for Pe = 1 and three values of Sc. Discontinuity in slope at $f = 1$, that is, $\omega = 2\Omega$ is a common feature caused by the change of sign in Eq. (2.9).

The effective convection–dispersion equation can be written in conservation form

$$\frac{\partial \hat{C}}{\partial T} + \frac{\partial \mathcal{F}_i}{\partial x_i} = 0, \qquad (5.40)$$

where

$$\mathcal{F}_i = U_{Ei}\hat{C} - (E_{ij} + D\delta_{ij})\frac{\partial \hat{C}}{\partial x_j} \qquad (5.41)$$

is the particle flux vector.

Under the present assumption of constant depth, the shore must be a vertical cliff normal to which there is no horizontal flux; that is,

$$\mathcal{F}_i n_i = \left[U_{Ei}\hat{C} - (E_{ij} + D\delta_{ij})\frac{\partial \hat{C}}{\partial x_{ij}}\right] n_i = 0. \qquad (5.42)$$

For presentation of numerical results, it is convenient to renormalize the variables as follows:

$$t = T'\frac{r_o^2\omega}{\mathcal{U}^2}, \qquad x_i = r_o x_i', \qquad \hat{C} = C'C_0$$

$$U_{Ei} = U'_{Ei}\frac{\mathcal{U}^2}{\omega r_o}, \qquad (D, E_{ij}) = \frac{\mathcal{U}^2}{\omega}(D', E'_{ij}), \qquad (5.43)$$

where the concentration scale depends on the problem to be specified later. The effective convection–diffusion equation then becomes

$$\frac{\partial \hat{C}'}{\partial T'} + \frac{\partial (U'_{Ei}C')}{\partial x_i'} = \frac{\partial}{\partial x_i'}\left((E'_{ij} + D'_h)\frac{\partial C}{\partial x_i'}\right) + \mathcal{E}'. \qquad (5.44)$$

In the following sections we shall limit our discussion to a semicircular peninsula. The first-order spatial dependence of the inviscid velocity field is then simple and is identical to that for uniform flow passing a circular cylinder

$$U_0 = \mathcal{U}U_0' = \mathcal{U}\left(1 - \frac{\cos 2\theta}{r'^2}\right),$$

$$V_0 = \mathcal{U}V_0' = -\mathcal{U}\left(\frac{\sin 2\theta}{r'^2}\right), \qquad (5.45)$$

where $r' = r/r_o$. The mean velocity of Eulerian streaming is shown for $f = 0.666$ in Fig. 4, showing a distinct asymmetry due to earth rotation and a convergence to a coastal region near $\theta = 135°$. In contrast, the mean streaming field in a nonrotating sea would be symmetrical with respect to the offshore (y) axis of the peninsula, with convergence toward the offshore tip of the peninsula (Lamoure and Mei 1977).

In Fig. 5 we display the Cartesian components of the dispersion tensor E_{ij} for the semicircular peninsula, for $f = 0.666$, Pe = Sc = 1. Again, the asymmetry is notable. For $f = 0$ these components are symmetrical with respect to the y axis, as shown in Fig. 6. For rough estimate let us take again $\mathcal{U} = 1$ m s^{-1} and $\omega = 1.45 \times 10^{-4}$ s^{-1}. From Fig. 2 the typical value of E_{ij} near the peninsula is 0.05, therefore the dispersivity is of the order $E_{ij} \sim 0.05\mathcal{U}^2/\omega = 345$ m^2 s^{-1}, which is consistent with the data cited by Zimmerman (1976a, b) and far greater than the eddy diffusivity.

In the following section we examine the spreading of a particle cloud for two examples. In the first a particle cloud is initially released into the bottom boundary layer near the peninsula; the surrounding sea bed is nonerodible. This is to simulate the fate of particles dumped into sea. In the second we examine the transport of sediments eroded from a strip of the sea bed surrounding the peninsula. The dimensionless horizontal diffusivity is taken to be $D'_h = 0.001$. For $\mathcal{U} = 1$ m s^{-1}, the physical diffusivity is $D_h = 6.9$ m^2 s^{-1}, which is about $350D$ and far smaller than the typical dispersivity to be discussed. The implied ratio ϵ_1 is much smaller than ϵ for an island of 10–100-km radius. Details of the numerical scheme are described in appendix B.

6. Release of a particle cloud

Let the initial concentration be Gaussian and the maximum initial concentration be chosen as C_0 for the scale of normalization. If the initial cloud has the dimensionless standard deviation S and is centered at x'_c, y'_c, then

$$C'(x', y', 0) = \exp\left\{-\frac{(x' - x'_c)^2 + (y' - y'_c)^2}{S^2}\right\}, \qquad (6.1)$$

where $x'_c = r'_c \cos\theta_c$, $y'_c = r'_c \sin\theta_c$. In all calculations we take $r'_c = 1.3$ and $S = 0.1$. The Coriolis factor is taken to be $f = 0.666$. Three locations of initial releases have been considered: $\theta_c = 45°$, 90°, and $\theta_c = 135°$. In each case the snapshots at $T' = 1$, $T' = 2$, $T' = 3$, and $T' = 4$ are plotted. Note that for Prom. del Gargano $r_o = 35$ km, $\mathcal{U} = 1$ m s^{-1} $\omega = 1.45 \times 10^{-4}$ s^{-1}. $T' = 1$ corresponds to 2.1 days. For comparison the tidal timescale is $1/\omega = 0.08$ day. Only the results for $\theta_c = 45°$ and 135° are shown here. In Fig. 7 we show the concentration contours when the initital cloud center is at $r'_c = 1.3$, $\theta_c = 45°$. At $T' = 1$ the initially concentric circular contours become tilted ellipses due mainly to the off-diagonal dispersivities (E_{xy} and E_{yx}). Some particles are transported toward the coastline around the point ($r' = 1$, $\theta = 45°$) as a result of both Eulerian convection and diffusion from the cloud center. Since the normal flux vanishes at the vertical shore, particles tend to pile against the shore, and the local radial gradient of the concentration reverses; that is, $\partial C/\partial r$ changes from positive to negative. Consequently, two local concentration peaks appear, one, designated as P_1, say, corresponds to the center of the initial cloud that is affected purely by convection, since the local concentration gradient is zero. The other peak corresponds to the accumulation along the coast, designated as P_2, say, and moves along the circular coastline. Note that at $T' = 1$, P_1 has not moved much from its original location owing to the small local convection velocity (cf. Fig. 7a). However, P_2 is displaced quite far from where the particle cloud first reaches the coast. More interesting is that P_2 passes the point where the Eulerian streaming converges around ($r' = 1$, $\theta = 135°$), instead of stopping there. To understand this phenomenon we express in polar form the component of particle flux along the circular coastline,

$$F_\theta = U_\theta C - E_{\theta r}\frac{\partial C}{\partial r} - \frac{E_{\theta\theta}}{r}\frac{\partial C}{\partial \theta}. \qquad (6.2)$$

The last term plays a small role in displacement of P_2 where $\partial C/\partial\theta$ vanishes. The second term on the right-hand side stands for the longshore flux due to the radial gradient, a result of the off-diagonal dispersivity $E_{\theta r}$. As shown in Fig. 8, $E_{\theta r}$ is positive along the entire rim of the island. Since $\partial C/\partial r$ is negative, the longshore flux is along the positive θ direction. Now the physical picture is clear:

1. When a peak is formed at the coastline due to local accumulation of particles, it is transported along the direction of increasing θ by both convection and diffusion.

2. When the peak of accumulation P_2 reaches the converging point of the convection field, the term representing off-diagonal dispersibity $E_{\theta r}\partial C/\partial r$ dominates and tends to move the peak P_2 past the point of velocity convergence. The clockwise convection velocity is too weak to counter the trend until the peak is finally stopped by the straight coastline.

From Figs. 7b–d it can be seen that P_1 moves from its original location (0.9, 0.9) in the x, y plane to about (0.8, 1.0). The concentration at P_2 increases with time due to additional accumulation of particles.

For other locations of initial release, the results are qualitatively the same [see Figs. 9a–d for initial release at ($r'_c = 1.3$, $\theta_c = 135°$)]. Thus, regardless of the different locations of initial release, the peak of the concentration cloud eventually reaches and stays around the stagnation point at $r' = 1$, $\theta = 180°$. Translating these results for Prom. del Gangano, we may

expect significant accumulation of suspended particles near the northwest corner, one or two weeks after dumping dredged mud somewhere nearby.

Along the equator the effects of earth rotation vanish since $f = 0$; the velocity field is symmetrical with respect to the y axis. Accordingly, the convection field and the dispersivity tensor are symmetrical with respect to the y axis. No matter where it is initially released, the cloud finally moves to the coastline and converges to the offshore tip of the peninsula. We only show in Fig. 10 the results for the case where the center is released at $r'_c = 1.3$, $\theta = 45°$. Thus, convection by Eulerian streaming, already predicted by Larmoure and Mei (1977), dominates the phenomenon, unlike the case with $f \neq 0$.

7. Erosion and transport of bottom sediments

We consider a peninsula surrounded by a ringlike strip of erodible seabed covering the region $r_0 < r < r_1$, $0° < \theta < 180°$. The bottom shear stress is dominated by the vertical derivative of the oscillatory horizontal velocity at $z = 0$, which can be evaluated from (Eqs. 2.4) and (2.5).

$$\begin{pmatrix} \tau_{bx} \\ \tau_{by} \end{pmatrix} = \begin{pmatrix} \mu \dfrac{\partial u^{(1)}}{\partial z} \\ \mu \dfrac{\partial v^{(1)}}{\partial z} \end{pmatrix}_{z=0}$$

$$= \frac{\mu}{2\delta} \mathrm{Re} \left\{ \begin{bmatrix} U_0(s+q) - iV_0(q-s) \\ iU_0(q-s) + V_0(s+q) \end{bmatrix} e^{-i\omega t} \right\}, \quad (7.1)$$

where q and s are defined in Eqs. (2.8) and (2.9). Limiting our discussion to $f = 2\Omega/\omega < 1$ only, it can be shown that

$$|\tau_b| = \sqrt{\tau_{bx}^2 + \tau_{by}^2}$$

$$= \frac{\mu}{\delta} \sqrt{U_0^2 + V_0^2} [1 - (1 - f^2)^{1/2} \sin 2\omega t]^{1/2}. \quad (7.2)$$

The time average over a wave period is

$$\langle |\tau_b| \rangle = \frac{\mu I}{2\pi\delta} \sqrt{U_0^2 + V_0^2} \quad (7.3)$$

in which I denotes the elliptic integral

$$I = 2 \int_0^{\pi} dt' \, [1 - (1 - f^2)^{1/2} \sin 2t']^{1/2}, \quad (7.4)$$

which can be evaluated numerically.

We now choose the concentration scale to be

$$C_0 = \frac{\mathrm{Pe} E \mu I \omega}{2\pi \mathcal{U}} \frac{r_o^2}{\delta^2} \quad (7.5)$$

so that the normalized erosion term on the right of (5.44) is

$$\mathcal{E}' = \begin{cases} \sqrt{U_o'^2 + V_o'^2}, & 1 < r' < r_1' \\ 0, & r' > r_1'. \end{cases} \quad (7.6)$$

Using Eq. (5.45), we find for the semicircular peninsula

$$\begin{cases} 0, & r' > r_1', \end{cases}$$

which is plotted for $r_1' = 1.5$ in Fig. 11. Note that this spatial variation is symmetrical with respect to the y axis and is unaffected by earth rotation because of the small size of the peninsula.

Computed results representing the evolution of the sediment concentration are shown for both $f = 0$ and $f = 0.666$. The corresponding elliptic integrals are $I = 5.65685$ and 6.12751 respectively.

As in the case of a nonerodible bed, once the particles are eroded from the bottom and resuspended, they drift toward the shore, resulting in a very sharp radial gradient. The concentration contours are asymmetrical with respect to y axis for $f \neq 0$ but symmetrical for $f = 0$, as expected. At large times, the peak of the resuspended sediment cloud moves past the region of velocity convergence and eventually settles around the stagnation point at $\theta = 180°$, if $f \neq 0$; see Fig. 12 for $f = 0.666$. Without rotation, however, the cloud settles around the point of velocity convergence; see Fig. 13.

Since the source term $\mathcal{E}'$ due to erosion is independent of time in our theory, the total mass in suspension increases with time at a constant rate.

8. Concluding remarks

Due to vertical shear in the bottom boundary layer, the effective diffusion in the horizontal direction is magnified. This magnification is very large since the tidal period is long, resulting in a dispersivity much greater than the eddy diffusivity. It should be stressed that the flow inside the boundary layer is determined by the flow above, which is in turn affected by bathymetry and coastline configuration. Therefore, the effective diffusivity and convection velocity are directly affected by the overall nonuniformity of the flow field and must, in general, vary from place to place. This means, in particular, that the dispersivity coefficients cannot be regarded as empirical constants to be calibrated by field measurements at a few stations.

For the special example of a semicircular peninsula we have found that the fate of a suspension cloud, whether it is released over a nonerodible bed or resuspended directly from an erodible bed, is determined jointly by the tide-induced circulation and dispersion. In general, for $f \neq 0$, the off-diagonal components of the dispersion tensor can overwhelm convection and drive the particle cloud to points away from where the convection velocity converges.

Several extensions of the present theory are desirable. First, for coastal applications, the combined effects of depth variation and wind input are vital. Wind can of course induce both currents and short gravity waves. As the depth decreases toward the shore, the influence of waves increases while that of the current must diminish due to bottom friction. Erosion must be largely the work of wind waves, while the transport of suspended particles is taken up by currents driven both directly by wind and indirectly by wave-induced currents through wave-induced Reynolds stresses (which are, of course, also the results of wind). Second, a more sophisticated turbulence model, calibrated by extensive field measurements, would bring predictions and observations closer. In particular, if the depth-dependent model (1.2) is used, the eddy viscosity itself would vary with the local flow and would affect the present predictions quantitatively. Third, very fine suspensions do not remain close to the bottom and can reach the upper layers of the sea. Knowledge of convection and dispersion throughout the entire depth of water is therefore needed. Fourth, due to sediment consolidation the erosion rate cannot remain unchanged in time (van Rijn 1993). The relation between erosion and consolidation is an unchartered territory of sediment dynamics and awaits detailed study. Finally for very fine sediments cohesive interactions such as floculation involve physicochemical processes beyond hydrodynamics; proper theories are true challenges for the future.

Acknowledgments

We are grateful for the financial support by the U.S. Office of Naval Research through Grant N00014-89-J-3128 with the Ocean Technology Program under Dr. Thomas Swean, and the U.S. National Science Foundation through Grant CTS 9634120 with the Fluid/Hydraulics/Particulates Program under Dr. Roger Arndt.

REFERENCES

Awaji, T., 1982: Water mixing in a tidal current and the effect of turbulence on tidal exchange through a strait. *J. Phys. Oceanogr.*, **12,** 501–514..

— ,N. Imasato, and H. Kunishi, 1980: Tidal exchange through a strait: A numerical experiment using a simple model basin. *J. Phys. Oceanogr.*, **10,** 1499–1508..

Bagnold, R. A., 1951: The movement of a cohesionless granular bed by fluid flow over it. *Brit. J. Appl. Phys.*, **2,** 29..

Batchelor, G. K., 1965: The motion of small particles in turbulent flow. *Proc. Second Australasian Conf. on Hydraulics and Fluid Mechanics.* Auckland, New Zealand, University of Auckland, 019–041..

Bowden, K. F., 1965: Horizontal mixing in the sea due to a shearing current. *J. Fluid Mech.*, **21,** 83–95..

— , 1967: Stability effects on mixing in tidal currents. *Phys. Fluids* (Suppl.), **10,** S278–S280..

— , and L. A. Fairbairn. 1952: A determination of the frictional forces in a tidal current. *Proc. Roy Soc.* London, **A214,** 371–392..

Buchwald, V. T., 1971: The diffraction of tides by a narrow channel. *J. Fluid Mech.,* **46,** 501–511..

Carter, H. H., and A. Okubo, 1965: A study of the physical processes of movement and dispersion in the Cape Kennedy area. Chesapeake Bay Inst., Johns Hopkins University Rep. 65-2, 150 pp..

Fang, G., and T. Ichiye, 1983: On the vertical structure of tidal currents in a homogeneous sea. *Geolp/hus. J. Roy. Astron. Soc.,* **73,** 65–82..

Fukuoka, S., 1974: A laboratory study on longitudinal dispersion in alternating shear flows. Res. Bull. No. 112, Dept. of English, James Cook University of North Queensland, Australia..

Geyer, W. R., and R. P. Signell, 1992: A reassessment of the role of tidal dispersion in estuaries and Bays. *Estuaries,* **15,** 97–108..

Holly, E. R., and D. R. F. Harleman, 1965: Dispersion of pollutants in estuary type flows. MIT Hydrodyn. Lab. Rep. 74, 202 pp. [Available from Dept. of Civil and Environmental Engineering, Massachusetts Institute of Technology, Cambridge, MA 02139.].

Huhe, O., and M. Q. Yang, 1996: Experimental study of the properties of cohesive sediment of the Yellow River Delta. (in Chinese). Rep., Institute of Mechanics, Chinese Academy of Sciences, Beijing, China, 39 pp..

Hunt, J. N., and B. Johns, 1963: Currents induced by tides and gravity waves. *Tellus,* **15,** 343–351..

Krone, R. B., 1962: Flume studies of the transport of sediment in estuarial shoaling processes. University of California Hydraulic Eng. and Sanitary Eng. Res. Lab. Berkeley, California, 110 pp..

Kundu, P. K., J. O. Blanton, and M. M. Jaunopaul, 1981: Analysis of current observations on the Georgia shelf. *J. Phys. Oceanogr.,* **11,** 1139–1149..

Lamoure, J., and C. C. Mei, 1977: Effects of horizontally two-dimensional bodies on the mass transport near the sea bottom. *J. Fluid Mech.,* **83,** 415–431..

Mei, C. C., and C. Chian, 1994: Dispersion of small suspended particles in a wave boundary layer. *J. Phys. Oceanogr.,* **24,** 2479–2495..

— , S. J. Fan, and K. R. Jin, 1997: Resuspension and transport of fine sediments by waves. *J. Geophys. Res.,* **102,** 15 807–15 821..

Mofjeld, H. O., 1980: Effects of vertical viscosity on Kelvin waves. *J. Phys. Oceanogr.,* **10,** 1039–1050..

Okubo, A., 1967: The effect of shear in an oscillatory current on horizontal diffusion from an instantaneous source. *Int. J. Oceanol. Limnol.,* **1,** 194–204..

— , 1971: Oceanic diffusion diagrams. *Deep-Sea Res.,* **18,** 789–802..

Patheniades, E., 1965: Erosion and deposition of cohesive soils. *J. Hydraul. Div. Amer. Soc. Civ. Eng.,* **91,** 105–139..

Signell, R. P., and W. R. Geyer, 1991: Transient eddy formation around peninsulas. *J. Geophys. Res.,* **96** (C2), 2561–2575..

Sleath, J. F. A., 1990: Seabed boundary layers. *The Sea:* Vol. 9(B), B. LeMehaute and N. M. Hanes, Eds., Wiley-Interscience, 693–727..

Soulsby, R. L., 1983: The bottom boundary layer in shelf seas. *Physical Oceanography of Coastal and Shelf Seas,* B. Johns, Ed., Elsevier, 189–266..

— , 1990: Tidal current boundary layers. *The Sea,* 9B. B. LeMehaute, and D. M. Hanes, Eds., McGraw Hill, 523–566..

van Rijn, L. C., 1993: *Principles of Sediment Transport in Rivers, Estuaries, and Coastal Seas.* Aqua Publ., A, 615 pp..

Sverdrup, H. U., 1927: Dynamics of tides on the northern Siberian shelf. 4. Geofys. Publ. Norske Videns, Acad. Oslo..

Yasuda, H., 1989: Longitudinal dispersion of suspended particles in oscillatory currents. *J. Mar. Res.,* **47,** 153–168..

Young, W. R, P. B. Rhines, and C. J. R. Garrett, 1982: Shear-flow dispersion, internal waves and horizontal mixing in the ocean. *J. Phys. Oceanogr.,* **12,** 515–527..

Yu, K. H., 1993: Preliminary study for the planning of Zhongshan Harbor, Jian Su Province (in Chinese). Internal Rep. 9406. Rivers and Harbors Res. Inst., Nanjing, China, 115 pp..

Zimmerman, J. T. F., 1976a: Mixing and flushing of tidal embayments in the western Dutch Wadden Sea. Part I: Distribution of salinity and calculation of mixing time scales. *Neth. J. Sea Res.,* **10** (2), 149–191..

— , 1976b: Mixing and flushing of tidal embayments in the Western Dutch Wadden Sea. Part II: Analysis of mixing processes. *Neth. J. Sea Res.,* **10** (2), 399–435..

— , 1977: Dispersion by tide-induced residual current vortices. *Hydrodynamics in Estuaries and Fjords,* Elsevier Oceanogr. Ser., 23, J.

C. J. Nihoul. Ed., Elsevier, 207–216..

— ,1986: The tidal whirlpool: A review of horizontal dispersion by tidal and residual currents. *Neth. J. Sea Res.*, **20,** 133–154..

APPENDIX A

9. List of Symbols

1. D eddy mass diffusivity
2. $\mathcal{D}$ rate of deposition
3. δ boundary layer thickness
4. E_{ij} effective dispersion tensor
5. $\mathcal{E}$ rate of erosion
6. ϵ ratio of tidal excursion to island radius
7. ϵ_1 ratio of boundary layer thickess to island radius
8. f $2\Omega/\omega$
9. $F_1,\ F_2,\ F$ vertical structures in the boundary layer
10. k wavenumber
11. n_i ith component of unit normal vector
12. ν_e eddy viscosity for momentum
13. Pe particle Péclet number
14. r radius in polar coodinates
15. Sc Schmitt number
16. θ angle in polar coordinates
17. $\mathbf{u}$ fluid velocity in the boundary layer
18. $\mathbf{U}$ fluid velocity above boundary layer
19. $\mathbf{u}^{(1)},\ \mathbf{u}^{(2)},\ \ldots$ Perturbation fluid velocity at the first, second, . . . , order
20. $\mathbf{U}_E$ Eulerian streaming velocity induced by Reynolds stresses
21. $x,\ y$ horizontal coordinates
22. z vertical coordinate from the sea bed
23. $\langle X \rangle$ time average of X over a wave period
24. $\overline{X}$ weighted depth average of X across the boundary layer.

APPENDIX B

10. The Numerical Scheme

We first split the dispersion tensor E_{ij} into symmetric D_{ij} and antisymmetric A_{ij} parts and rewrite the governing equation in the following form:

$$\frac{\partial C}{\partial t} + u'\frac{\partial C}{\partial x} + v'\frac{\partial C}{\partial y} + \gamma C = D_{xx}\frac{\partial^2 C}{\partial x^2} + D_{yy}\frac{\partial^2 C}{\partial y^2} + 2D_{xy}\frac{\partial^2 C}{\partial x \partial y}, \quad \text{(B.1)}$$

where

$$u' = U_{E_1} + \frac{\partial A_{xy}}{\partial y} - \frac{\partial D_{xx}}{\partial x} - \frac{\partial D_{xy}}{\partial y}, \quad \text{(B.2)}$$

$$v' = U_{E_2} - \frac{\partial A_{xy}}{\partial x} - \frac{\partial D_{xy}}{\partial x} - \frac{\partial D_{yy}}{\partial y}, \quad \text{(B.3)}$$

$$\gamma = \frac{\partial U}{\partial x} + \frac{\partial V}{\partial y}. \quad \text{(B.4)}$$

These are then transformed in polar coordinates,

$$\frac{\partial C}{\partial t} + u'_r\frac{\partial C}{\partial r} + u'_\theta\frac{\partial C}{r\partial \theta} + \gamma C = D_{rr}\frac{\partial^2 C}{\partial r^2} + D_{\theta\theta}\frac{\partial^2 C}{r^2\partial \theta^2} + 2D_{\theta r}\frac{\partial^2 C}{r\partial\theta\partial r}, \quad \text{(B.5)}$$

with

$$u'_r = u'\cos\theta + v'\sin\theta - \frac{D_{xx}}{r}\sin^2\theta - \frac{D_{yy}}{r}\cos^2\theta + \frac{D_{xy}}{r}\sin 2\theta, \quad \text{(B.6)}$$

$$u'_\theta = -u'\sin\theta + v'\cos\theta - \frac{1}{r}(D_{xx}\sin 2\theta + D_{yy}\sin 2\theta + 2D_{xy}\cos 2\theta), \quad \text{(B.7)}$$

$$D_{rr} = D_{xx}\cos^2\theta + D_{yy}\sin^2\theta + D_{xy}\sin 2\theta, \quad \text{(B.8)}$$

$$D_{\theta\theta} = D_{xx}\sin^2\theta + D_{yy}\cos^2\theta - D_{xy}\sin 2\theta, \quad \text{(B.9)}$$

$$D_{\theta r} = \frac{1}{2}\sin 2\theta(D_{yy} - D_{xx}) + D_{xy}\cos 2\theta. \quad \text{(B.10)}$$

As the radial variation near the peninsula is expected to be very rapid, we introduce the stretching: $r = \exp(2\pi\zeta)$ and $\eta = \theta/\pi$ so that Eq. (B.5) becomes

$$D_{\zeta\zeta}\frac{\partial}{\partial\zeta^2} + D_{\eta\eta}\frac{\partial}{\partial\eta^2} + 2D_{\zeta\eta}\frac{\partial}{\partial\zeta\partial\eta}, \quad \text{(B.11)}$$

where

$$u_\zeta = u'_r s_0 + 2\pi s_0^2 D_{rr}, \qquad u_\eta = 2u'_\theta s_0, \quad \text{(B.12)}$$

$$u_\eta = 2u'_\theta s_0, \quad \text{(B.13)}$$

$$D_{\zeta\zeta} = s_0^2 D_{rr}, \qquad D_{\eta\eta} = 4s_0^2 D_{\theta\theta}, \qquad D_{\zeta\eta} = 2s_0^2 D_{r\theta}, \quad \text{(B.14)}$$

and

$$s_0 = \frac{1}{2\pi r}. \quad \text{(B.15)}$$

The alternating direction implicit scheme is unconditionally stable and allows us to use reasonably large time steps with second-order accuracy. A second-order approximation for the normal derivative is employed for the no-flux boundary condition on the coast.

As a confirmation of numerical accuracy, we check that total mass is conserved in the nonerosion case:

$$\begin{aligned} M = M_0 &= \int\int C(x, y)\, dx\, dy \\ &= \int\int C(r, \theta) r\, dr\, d\theta \\ &= \int\int C(\xi, \eta) e^{2\pi\xi} |J|\, d\xi\, d\eta, \end{aligned} \quad \text{(B.16)}$$

where the Jacobian determinant is given by

$$|J| = \frac{\partial(r, \theta)}{\partial(\zeta, \eta)} = 2\pi^2 r. \quad \text{(B.17)}$$

With time marching, the computed total mass, however, increases slightly due mainly to the temporal accumulation of numerical errors and the inaccuracy in numerical integration for the total mass. The improvement of numerical accuracy by denser grids is shown here where the relative mass increase is shown at a certain time after an initial release at a particular location.

Tables

Table 1B. Dependence of numerical accuracy on density of grids.

Mesh density		200 × 200	400 × 200
$\theta_c = 45°$	$T = 2$	4.0%	0.92%
	$T = 4$	11.8%	3.0%
$\theta_c = 135°$	$T = 2$	5.3%	1.3%
	$T = 4$	8.3%	2.1%

Click on thumbnail for full-sized image.

Figures

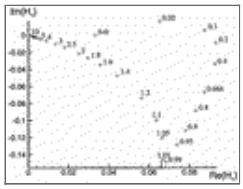

Click on thumbnail for full-sized image.

Fig. 1. Dimensionless complex coefficient H_1 (f, Pe) for the mean convection velocity as a function of Coriolis number $f = 2\Omega \sin \Phi/\omega$ for Pe = 1.

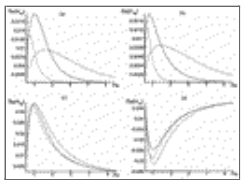

Click on thumbnail for full-sized image.

Fig. 2. Dimensionless dispersivity coefficients as functions of Pe for f = 0.666. Dash: Sc = 0.1, solid: Sc = 1 and, dash–dot: Sc = 10.

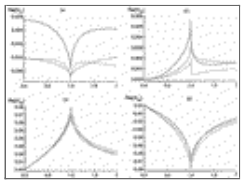

Click on thumbnail for full-sized image.

Fig. 3. Dimensionless dispersivity coefficients as functions of f for Pe = 1. Dash: Sc = 0.1, solid: Sc = 1, and dash–dot: Sc = 10.

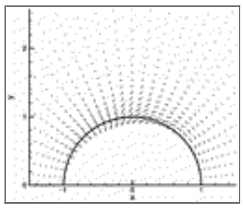

Click on thumbnail for full-sized image.

Fig. 4. Weighted depth average of convection velocity $\mathbf{U}_E$ in tidal boundary layer for f = 0.666 and Pe = 1.

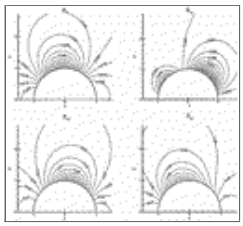

Click on thumbnail for full-sized image.

Fig. 5. Dispersivity tensor components around a circular peninsula for f = 0.666, Pe = 1, and Sc = 1.

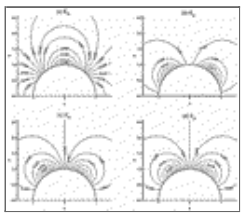

Click on thumbnail for full-sized image.

Fig. 6. Dispersivity tensor components around a circular peninsula for f = 0, Pe = 1, and Sc = 1.

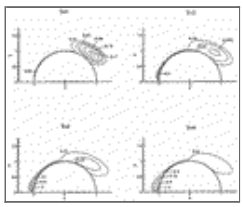

Click on thumbnail for full-sized image.

Fig. 7. Evolution of particle concentration. Cloud center is initially released at northeast (r'_c = 1.3, θ_c = 45°) for f = 0.666, Pe = 1, and Sc = 1.

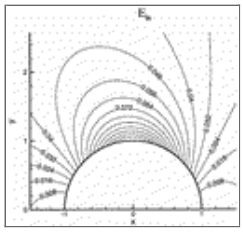

Click on thumbnail for full-sized image.

Fig. 8. Off-diagonal dispersivity tensor component $E_{\theta r}$ around a circular peninsula for f = 0.666, Pe = 1, and Sc = 1.

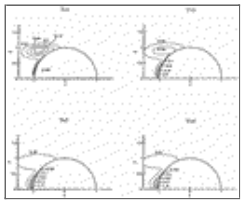

Click on thumbnail for full-sized image.

Fig. 9. Evolution of particle concentration. Cloud center is initially released at northwest (r'_c = 1.3, θ_c = 135°) for f = 0.666, Pe = 1, and Sc = 1.

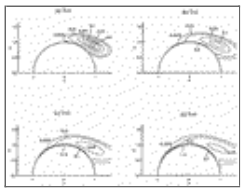

Click on thumbnail for full-sized image.

Fig. 10. Evolution of particle concentration. Cloud center is inititally released at northeast (r'_c = 1.3, θ_c = 45°) for f = 0, Pe = 1, and Sc = 1.

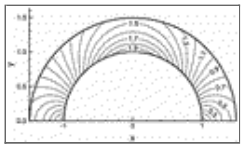

Click on thumbnail for full-sized image.

Fig. 11. Dimensionless erosion rate around a circular peninsula due to tidal oscillations.

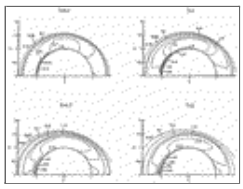

Click on thumbnail for full-sized image.

Fig. 12. Evolution of concentration of resuspended particles. For f = 0.666, Pe = 1, and Sc = 1. Dash curve indicates outer edge of erodible bed.

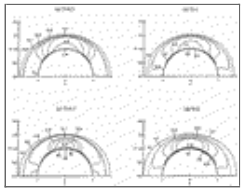

Click on thumbnail for full-sized image.

Fig. 13. Evolution of concentration of resuspended particles for f = 0, Pe = 1, and Sc = 1. Dash curve indicates outer edge of erodible bed.

Corresponding author address: Dr. Chiang C. Mei, Department of Civil and Environmental Engineering, Ralph M. Parsons Laboratory, Room 1-353, Massachusetts Institute of Technology, Cambridge, MA 02139.

E-mail: ccmei@mit.edu

[1] These and other mathematical symbols are summarized in appendix A.

[2] For reference, the shape of Prom. del Gargano is not too far from a semicircle with a radius of 35 km. The 50-m depth contour is about 20 km offshore. The coastline extends from northwest to southeast.

top